Ecological Modelling 387 (2018) 70–82

Contents lists available at ScienceDirect

Ecological Modelling

journal homepage: www.elsevier.com/locate/ecolmodel

A hydrodynamic analytical model of fish tilt angle: Implications regarding acoustic target strength modelling

F. Agustín Membiela, Matías G. dell'Erba*

IFIMAR (CONICET and Universidad Nacional de Mar del Plata), Deán Funes 3350, B7602AYL Mar del Plata, Argentina

ARTICLE INFO

Keywords:
Hydrodynamic analytical model
Fish tilt angle
Acoustic target strength
Physostomous fish

ABSTRACT

We implement a simple hydrodynamical model to study the behavioural swimming tilt angle of open swimbladder fish. For this purpose we analysed the force stability which act upon a fish swimming horizontally at a constant velocity. Furthermore, the open swimbladder compression at depth is modelled by Boyle's law. With these, our model gives us an analytical solution relating depth with body tilt angle and velocity. An interesting result that surges from steady horizontal swimming is that the body tilt decreases with velocity almost like v^{-1}. Moreover, we provide an expression for the tilting as function of depth that asymptotically yields the maximum tilt angle. Additionally, by introducing the assumption of constant swimming power we can relate the swimming velocity to the tilting. We also show that the hydrodynamical influence of a temperature gradient produced by a thermocline does not seem to affect fish tilting significantly. Finally, we obtain reasonable results by comparing our hydrodynamics solutions with acoustic observations and simulations obtained from of Target Strength simulations of Argentine anchovy *(Engraulis anchoita)*.

1. Introduction

The study, control and protection of marine ecological resources is carried out in part by *in situ* acoustic measurements. Therefore, in order to achieve a deeper understanding of marine environment, it is necessary to generate more accurate measurements and, at the same time, acoustic models that correctly interpret the data obtained. In Hazen and Horne (2003) it has been shown that the acoustic measurements of fish are strongly influenced by the angle of swimming, more than by size. Consequently, it would be of importance to estimate the swim tilt from a hydrodynamic model, dependent on observable variables such as depth or swim speed and anatomical parameters such as swimbladder volume, fins area, etc.

Teleost fish use their swimbladders to regulate buoyancy. Regarding this, they could be divided into two groups; physoclists, with a closed swimbladder and physostomes, with an open swimbladder (Morrissey et al., 2016; Gilles, 1991). The physoclist fish has a gas secretion system connected to its bloodstream system through which it can adjust the swimbladder pressure and volume, thus allowing it to keep close to neutral buoyancy for different depths. On the other hand, the physostomous fish, that posses a more primitive morphology, are incapable of refilling their swimbladders like physoclist. Instead, their swimbladders only seem to be refilled by 'gulping' atmospheric air from the surface (Blaxter and Hunter, 1982; Blaxter and Batty, 1984; Brawn, 1962).

It is well-known, regarding ecological acoustics, that the primary reflection of acoustic energy happens at the swimbladder (Foote, 1980a,b). Moreover, fish with swimbladders that are comparable or longer than the wavelength are acoustically directive. Thus, small changes in the tilt of the fish can affect significantly the measured target strength (TS, dB re 1 m^2). Indeed, an incorrect estimation of behavioural tilt angle distribution may spoil the determination of biomass from echoenergy integration. The variation of TS as a function of tilt angle has been extensively studied (Foote, 1980a,b; Huse and Ona, 1996; Nakken and Olsen, 1977; McQuinn and Winger, 2003; Prario et al., 2015; Kang et al., 2005). On the other hand, it was suggested that negatively buoyant fishes may opt for a positive body tilt during steady horizontal swimming as a behavioural mechanism to avoid sinking (Huse and Ona, 1996; He and Wardlet, 1986; Wilga and Lauder, 2000). In turn, in Strand et al. (2005), they discussed the energy saving obtained through fish swimming tilt angle by physoclist fish.

The theoretical modelling of fish target strength involves previous knowledge of fish behaviour, i.e., the tilt angle distribution of fish. This is necessary to properly average target strength functions over a certain tilt angle distribution. However, this knowledge is obtained with considerable difficulty since direct observations of fish swimming tilt angle are rather scarce. This is particularly so when TS models aim is to provide a deeper insight into the acoustical scattering of the organisms in the wild, which in turn constitutes a major concern for acoustic

* Corresponding author.
E-mail addresses: agustinmembiela@gmail.com (F.A. Membiela), mdellerba@ifimar-conicet.gob.ar (M.G. dell'Erba).

https://doi.org/10.1016/j.ecolmodel.2018.05.022
Received 6 September 2017; Received in revised form 8 May 2018; Accepted 24 May 2018

assessment surveys. In this respect we aim to develop a simple model of the fish swimming that can be used to estimate the "expected" tilt angle adopted by a specific fish species. We took into consideration the influence of certain external factors concerning fish behaviour and we concentrate on the particular example of physostomous fish, which, because of the way it regulates buoyancy, frequently performs vertical migrations in the water column and hence is exposed to a significant variation of hydrostatic pressure and the consequential effects on its buoyancy conditions. The specific anatomy of fish is taken into account in order to provide an approximate but more realistic source for estimating the average tilt angle of fish. In this way we expect to narrow the subjectivity usually associated to the selection of fish tilt angle pdf's for averaging TS functions.

Several authors have studied fish swimming focusing particularly on the hydrodynamics of undulatory propulsion generation (Sfakiotakis et al., 1999; Shadwick and Lauder, 2006). Today, the preferred simple analytical model of fish swimming kinematics is Sir J. Lighthill's elongated body theory (Lighthill, 1960, 1971), which is based on addition of forces due to the lateral acceleration and deceleration of the body as it undulates from side to side.

Our main goal is to develop a simple model to estimate the behavioural tilt angle of physostomous fish. In turn, this may be easily extended to physoclists and negative buoyant fish without swimbladder. Specifically, we have chosen simplified swimming behaviour by assuming a steady horizontal trajectory, in contrast to other swimming strategies, like *glide and rise*, which may be adopted for deeper depths (Huse and Ona, 1996; Tanaka et al., 2001). With this treatment we are not intended in giving a comprehensive cover of fish swimming, instead, we are interested in developing a new model of swimming tilt angle by studying simple hydrodynamics of the body and the pectoral fins, independently of the propulsion movements and thrust generation, so as to obtain general results within a few parameters. With this approach we shall obtain analytical expressions for the tilt angle of fish swimming, that may offer a wider insight, and should be easily applicable to a variety of species. However, the model still suffers from lack of validation with experimental (e.g., flume tank experiments) and in situ optical data.

By means of physiological and hydrodynamical arguments, we will try to shed some insight on the relation between the tilt angle, the swimming depth and the swim velocity of physostomous fish that suffer loss of buoyancy because of swimbladder compression with depth. This will help on the construction of simulations of individual TS and volume scattering of fish schools.

We are presenting the paper in the following manner. In Section 2, we are introducing the hydrodynamical model from which we obtain a simplified equation relating the tilting angle with depth and swimming velocity. In turn, we add a constant swimming power hypothesis which yields a tilting dependence, due to velocity. Additionally, we take into consideration the effects of the presence of a thermocline in the model. In Section 3, we test our model against acoustic data and simulations of TS Argentine anchovy *(Engraulis anchoita)*. Finally, in Section 5 we discuss the results and submit our conclusions.

2. The hydrodynamical model

We are studying the hydrodynamic vertical stability of a fish swimming at a stationary velocity and depth. For this purpose we consider the different forces acting upon the fish components (fins, body, etc.). In this approach we will ignore constraints introduced by bioenergetic costs and the efficiency of buoyancy regulation during swimming. This last common bioenergetics framework has been modelled by Strand et al. (2005) for physoclists, by including the trade-offs between the swimbladder regulation and the hydrodynamics forces.

Furthermore, fish are self-propelled by undulatory movements, thus it is hard to separate thrust generation from their inherited drag forces (Schultz and Webb, 2002). However, if we assume that these movements are confined to a reduced portion of the posterior fish body and/or the caudal fin, then we can approximate the fish body as a rigid body. Indeed, in such cases we can consider that the fish body behaves, in a hydrodynamic manner, similar to a torpedo-shaped body travelling with a definite tilt angle (Jorgensen, 1973; Evans, 2003). In this way, we take into consideration the simplification that the interactions between the fluid and the fish body are independent of the thrust generating undulatory movements. Such simplified approach was also chosen by Strand et al. (2005).

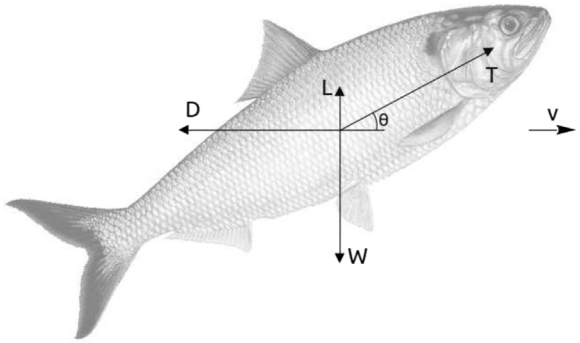

Fig. 1. Forces acting on a fish during horizontal swim with velocity v: **T**, the thrust force in the direction θ; **W**, the apparent weight; **L**, the total lift force, and **D** the total drag force.

2.1. Forces during stationary swimming

In Fig. 1 we summarized the forces acting upon the fish while swimming horizontally with a velocity v (in body length per second, ℓ/s) and tilt θ (in degree, °). The thrust force **T** (all forces in newtons, N) is the consequence of the propulsion obtained from the specific fish swimming mode. In the carangiform and the thunniform swimming modes the thrust is obtained from the body and caudal fin, thrown into a wave with as much as up to one half-wavelength along the length of body (Webb, 1975). Indeed we expect that our study may only be limited to these undulatory modes. On the other hand, swimming with stationary velocity and depth, determines particular behaviour or swimming strategy given by stationaries tilt and thrust. Other swimming strategies can be studied where the tilt and thrust are not constant (Videler, 1993; Taylor et al., 2010; Sfakiotakis et al., 1999).

The apparent weight **W** is a force that always appears on submerged bodies, which is the resultant between the Archimedes force and the weight of the fish. This force changes with depth as the swimbladder compresses. If the fish has negative apparent weight at the surface (with **W** pointing upwards), it means that floats on water, then in order to gain depth it will need to nose downwards with a negative tilt angle. Eventually, at a certain depth the average fish density equals the water density reaching the neutral buoyant depth. However, this is an unstable point since below of this depth **W** changes sign, pointing downwards and the fish starts to sink. Then, for the fish to swim at a constant depth, this positive apparent weight should be compensated by some other vertical forces. Essentially there will be two kinds, lift forces and the vertical component of the thrust force for a swimming tilt angle. Hydrodynamical lift **L** while swimming may be obtained mainly from pectoral fins acting as hydrofoils and from body lift. Additionally, hovering behaviour may be used but in this case the fish is not moving and cannot be combined with the other forces. Finally, the drag forces **D**, that always oppose to the flow direction, manifest as pressure drag and friction drag.

There is an extensive bibliography on the study of the hydrodynamics (and aerodynamics) acting either on biological creatures or engineering systems (Webb, 1975, 1988; Vogel, 1996; Norberg, 1990; FAA, 2012; McNeill, 1982).

The steady motion assumption implies that all forces balance, thus

there is no acceleration. From Newton laws we obtain,

$$L - W + T\sin\theta = 0 \tag{1}$$

$$T\cos\theta - D = 0, \tag{2}$$

where θ is the angle between oblique thrust **T** and horizontal velocity **v**. We can combine both equations to get,

$$W = L + D\tan\theta. \tag{3}$$

In this paper we shall keep as simple as possible and we shall ignore the moments stability analysis. However, a more detailed study on particular fish species should incorporate this issue.

2.2. Swimbladder and body compression

Some of the strategies of Nature to achieve buoyancy are the lipid (or oil) reservoirs in the fish flesh, which help to reduce the averaged fish density ρ_b (all densities in kg/m^3) (Shadwick and Lauder, 2006; Alexander, 1990). In turn, other fish posses the gas-filled swimbladder organ that aims to the same purpose. We shall consider that the open swimbladder follows Boyle's Law contraction rate (Gorska and Ona, 2003; Nero et al., 2004) which means that

$$V_{sb}(z) = V_{sb0}\left(1 + \frac{\rho g}{P_0}z\right)^{-1} \tag{4}$$

where z (in m) is the depth below water surface, $V_{sb}(z)$ is the swimbladder volume at a depth z (with $V_{sb}(0) = V_{sb0}$), ρ is the water density, g (in m/s^2) is the gravity acceleration and P_0 (in N/m^2) is the atmospheric pressure at sea level. Moreover, we assume that the mean flesh density is practically constant in spite of the swimbladder contraction with the depth. Thus, the loss of volume by the swimbladder is followed by an equal loss of external volume in the fish body $V_{sb}(z) - V_{sb0} = V_b(z) - V_{b0}$,where $V_b(z)$ is the volume of the entire fish at depth z. Using these considerations, we obtain an expression for the apparent weight depth dependence,

$$W(z) = (\rho_b - \rho)g(V_{b0} - V_{sb0}) - \rho g V_{sb0}\left(1 + \frac{z}{z_*}\right)^{-1}, \tag{5}$$

where ρ_b is the mean fish density and $z_* = P_0/(\rho g) \simeq 10$ m, is a reference depth at which the swimbladder shrinks to half the volume from the sea level value V_{sb0}. Thus, the apparent weight increases hyperbolically from

$$W_0 = (\rho_b - \rho)gV_{b0} - \rho_b g V_{sb0}, \tag{6}$$

at sea level ($z = 0$), to deep values where the swimbladder is totally collapsed

$$W_\infty = (\rho_b - \rho)g(V_{b0} - V_{sb0}), \tag{7}$$

for $z \gg z_*$. The difference between these values is $W_\infty - W_0 = \rho g V_{sb0}$. We can further define the *neutral buoyancy depth* z_N obtained from the condition $W(z_N) = 0$. It is easy to see that,

$$z_N = -z_*\frac{W_0}{W_\infty}. \tag{8}$$

As a consequence, when the fish flesh is denser than the sea water, $W_\infty > 0$ and then in order to obtain positive buoyancy, $W_0 < 0$.

2.3. Tilting depth dependence

By combining Eq. (3) with (5) we obtain

$$z(\theta, v) = z_*\left(\frac{1}{F(\theta, v) + f_0} - 1\right), \tag{9}$$

where we have defined,

$$F(\theta, v) = -\frac{D(\theta, v)\tan\theta + L(\theta, v)}{\rho g V_{sb0}} \simeq v^2 f_1(\theta), \tag{10}$$

$$f_0 = \left(\frac{\rho_b}{\rho} - 1\right)\left(\frac{V_{b0}}{V_{sb0}} - 1\right). \tag{11}$$

Eqs. (9)–(11) are the main results of the paper, they give the depth at which the forces on the fish balance, for a steady horizontal swimming with velocity v and tilting θ. In Appendix A we present some expressions for the estimation of **D** and **L** forces and we discuss the validity of the factorization $v^2 f_1(\theta)$ in Eq. (10). It is not possible, though, to obtain an exact analytical expression $\theta = \theta(z, v)$ from Eq. (9). Still, we have checked that $f_1(\theta)$ behaves practically like a quadratic function in the range of studied parameters, therefore, by keeping to order θ^2 in the power expansion of $f_1(\theta)$ we obtain

$$f_1(\theta) \simeq -\frac{1}{2gV_{sb0}}[2(S_f k + A_s + 5\eta A_p R_{2r}^{-2/3})\theta + \overline{C}_\perp A_p \theta^2], \tag{12}$$

where the parameters in the expansion are detailed in Appendix A. Using Eqs. (9)–(12)) we can solve the tilting angle depth dependence

$$\theta(z, v) \simeq \frac{S_f k + A_s + 5\eta A_p R_{2r}^{-2/3}}{A_p \overline{C}_\perp} \times \left\{\sqrt{1 + \frac{2gV_{sb0}A_p\overline{C}_\perp}{(S_f k + A_s + 5\eta A_p R_{2r}^{-2/3})^2}\left[\left(\frac{\rho_b}{\rho} - 1\right)\left(\frac{V_{b0}}{V_{sb0}} - 1\right) - \frac{z_*}{z_* + z}\right]\frac{1}{v^2}} - 1\right\}. \tag{13}$$

In Fig. 2 we compare the functions $z(\theta)$ from the exact expression Eq. (9) (solid line) with the approximation from Eq. (13) (dashed line) for swimming velocities $v[\ell/s] = 1.0, 1.5, 2.0$ and fish flesh density $\rho_b[\text{kg/m}^3] = 1060$. We also assumed absence of lift from pectoral fins ($k = 0$), thus all the hydrodynamic lift comes from body lift. The parameters used from now on correspond to a representative specimen of Argentine anchovy and they are given in the table of Section 3.1, unless stated otherwise. We remark that the approximation is good within a maximum error of about 1° for $v \sim 1\ell/s$.

Firstly, we can identify that, for a fish flesh density $\rho_b = 1060$ kg/m^3, neutral buoyancy is achieved near the sea surface. Indeed, all constant velocity curves will generally meet at $z = z_N$, because nevertheless the velocity and to keep horizontal swimming, at that depth there is no need of any lift forces. Hence, the body tilting will remain zero. Of course, this situation occurs whenever there is no lift happening at the pectoral fins or any asymmetry in the body shape that can either generate any lift force at zero angle of attack.

It is immediate to see that the tilting θ increases with depth to a

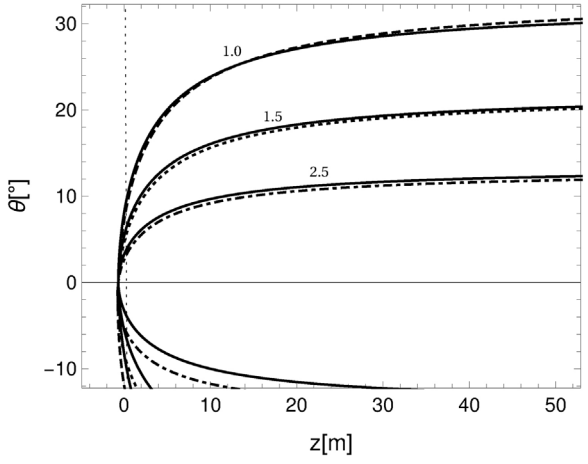

Fig. 2. z[m] vs. $\theta[deg.]$ from (9) (solid) and with the approximation (13) (dashed, dotted and dot-dashed) for body density $\rho_b = 1060$ kg/m^3, $k = 0$ and velocities $v = 1.0\,\ell$/s, $v = 1.5\,\ell$/s and $v = 2.5\,\ell$/s. The vertical dot line is the sea surface level.

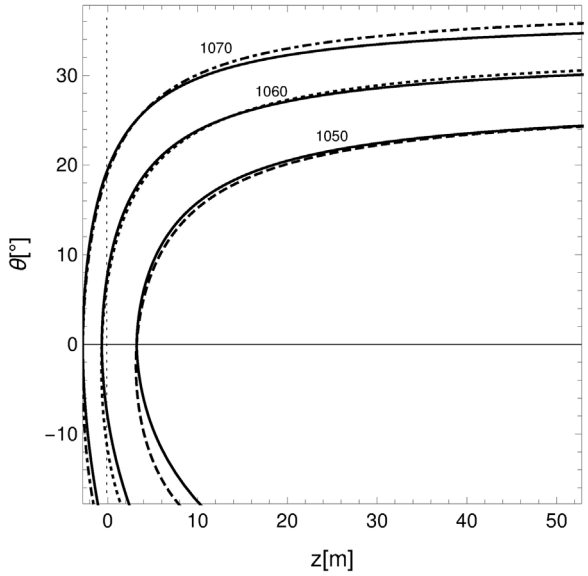

Fig. 3. z[m] vs. θ[*deg.*] from (9) (solid) and with the approximation (13) (dashed, dotted and dot-dashed) for velocity $v = 1.0\ell$/s, $k = 0$ and densities $\rho_b = 1050$kg/m^3, $\rho_b = 1060$kg/m^3 and $\rho_b = 1070$kg/m^3. The vertical dot line is the sea surface level.

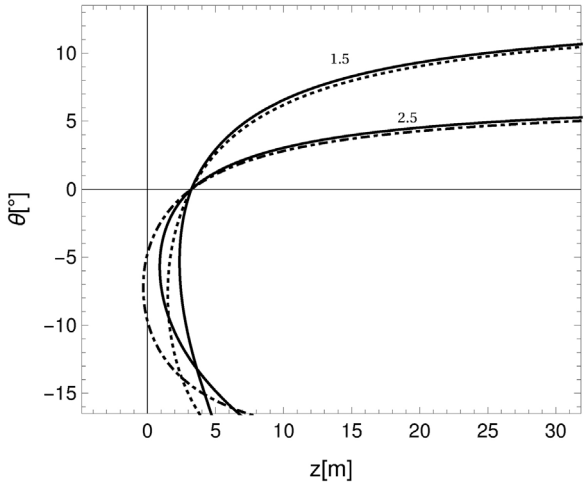

Fig. 4. z[m] vs. θ[*deg.*] from (9) (solid) and with the approximation (13) (dotted and dot-dashed) for body density $\rho_b = 1050$kg/m^3, $k = 2\pi$ and velocities $v = 1.5\ell$/s and $v = 2.5\ell$/s.

maximum asymptotic value $\theta_{\max}$ as $z \gg z_*$. The value of $\theta_{\max}$ is given by this last expression without the z-dependent term. The tilting decreases at an approximate rate $\sim v^{-1}$ as could be seen in Eq. (13). This happens because the main contribution comes from θ^2 term in Eq. (12) that belongs to the planform area of the fish. This result is in concordance with experimental fits $\theta(v) \propto v^{-1.14}$ obtained for trout in Webb (1993) through flume tanks experiments. In this way, the faster the fish swims the less tilt it needs to achieve stability, because at faster movement the lift forces grow, allowing to reach the body stability with less tilt (Fig. 2) (He and Wardlet, 1986; Svendsen et al., 2005). Otherwise, the tilting will be enhanced for denser fishes, because an extra component of vertical thrust is needed to cancel the extra weight. This should be evident in Fig. 3 where tilting curves are plotted for different densities ρ_b[kg/m^3] = 1050, 1060, 1070 and $v[\ell/s] = 1.0$. Thus, we can see how for more negative buoyant fish the body tilt angle of attack at the sea surface increases. In particular, for a flesh density 1050 kg/m^3 the buoyancy at surface is positive because the averaged density of the fish including the swimbladder is lower than the water density. In this case the fish should either swim with negative tilt or lose some air of the swimbladder to keep stable. In Fig. 3 we see that the curve cannot reach the surface, even if swimming with negative tilt angle, this means that there is no hydrodynamic solution for the fish to maintain a horizontal swim under such circumstances. Anyway, the fish could either shift to oblique swimming to reach sea surface, or use negative angle of attack of pectoral fins to achieve the needed negative lift. This situation becomes clear in Fig. 4, in this case we considered pectoral fins lift $k = 2\pi$, so for negative angles the tilt curve could reach $z = 0$.

2.4. Constant swimming power assumption

The swimming power developed by the fish is $P = \mathrm{Tv}\cos\theta$. Thus, by using Eq. (2) we get $P = \mathrm{Dv}$ and by assuming a constant swimming power (CSP) we can obtain an equation that relates the horizontal velocity with the tilt angle,

$$D(\theta, v)v = D(0, v_0)v_0 = \mathrm{cte}, \tag{14}$$

where we have established a constant power defined by the reference value $\theta = 0°$ and its *reference velocity* v_0, the maximum horizontal velocity. This expression introduces a restriction between the behavioural variables θ and v that is explicitly independent of the depth z. It is also important to note that given that the drag coefficient depends on the velocity (see Appendix A), this equation is transcendental in v and should be solved by numerical methods.

As we can see in the right plot of Fig. 5, the maximum velocity is obtained for $\theta = 0$ where all the power developed is spent on moving, whilst when swimming with tilt angle a fraction of the power is used to keep at a certain depth.

Previously we discussed in Section 2.3 that there exists an asymptotic $\theta_{\max}(v)$ for $z(\theta, v)$ in Eq. (13). In the CSP context, this corresponds with an asymptotic decrease of the horizontal velocity with the depth up to a minimum, $v_{\min}$ (see left plot of Fig. 5). In turn, the velocity also decays monotonically with the body tilt as in (Wilga and Lauder, 2000; Nowroozi et al., 2009; Svendsen et al., 2005; Webb, 1975). In the right plot of Fig. 5 we marked the intersections of the curves $v(\theta)$ with the curve $\theta_{\max}(v)$ that determine the asymptotic minimum velocities $v_{\min}$ for given v_0 in the CSP model. Therefore, the curves to the right of the intersection points have no physical sense.

The recordings made for herrings at night by Huse and Ona (1996) support our results. In this case, instead of increasing swimming speed, the fish adopted a swimming tilt angle strategy. Moreover, the observed velocities were slower at deeper depths and vice versa.

We would like to remark that we are considering a stationary horizontal swimming strategy and that another swimming strategy (e.g. glide and rise) could give slower or faster velocities than this model.

2.5. Effects of other environmental factors: the thermocline

In this section we consider the effects on fish buoyancy that could be triggered by a sharp change in physical parameters of water column. The particular case of a strong temperature gradient is analyzed but similar results could be expected by strong gradients on the salinity and thus affecting water density in a similar way.

From Eq. (13) it can be seen that the fish tilt angle depends on both 'physiological' and 'environmental' sets of parameters. As examples of the first set are the body area A, the flesh density ρ_b, the swimbladder volume on surface V_{sb0}, etc. We consider these parameters constant for a specific fish specimen. In the second set are for example the water density ρ and water viscosity μ, both of which are temperature dependent (Talley et al., 2011; IOC, 2010). The region of higher vertical temperature gradient in the column of seawater is called the *thermocline*. At this place, the temperature decreases rapidly from the mixed layer temperature (roughly that of surface water) to the colder deep water temperature. We want to quantify how much fish tilt swim would be affected from the hydrodynamics by the variation of the

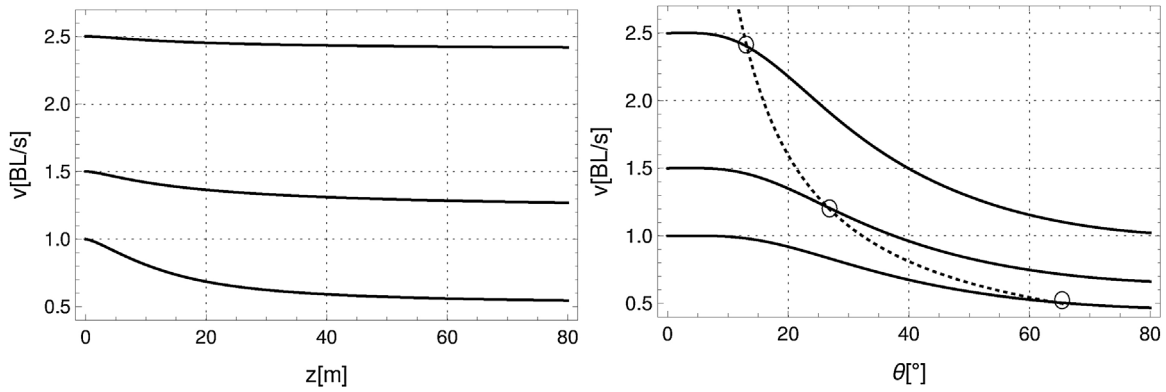

Fig. 5. Left plot: $v\,[\ell/\mathrm{s}]$vs. $z\,[\mathrm{m}]$ for the CSP hydrodynamic model with velocities $v_0\,[\ell/\mathrm{s}] = 2.5, 1.5, 1.0$. Right plot: $v\,[\ell/\mathrm{s}]$vs.$\theta\,[deg.\,]$ for the CSP hydrodynamic model with velocities $v_0\,[\ell/\mathrm{s}] = 2.5, 1.5, 1.0$. The dashed curve corresponds to $\theta_{\max}(v)$. The intersections marked with circles correspond to the asymptotic velocities.

environmental parameters with temperature.

Although the water density and the water viscosity change with the temperature, in the usual thermocline temperature range, the viscosity variation introduces negligible changes in the final result (see discussion of $\overline{C_\perp}$ in (A.1.1)). Hence, the primarily temperature contribution will come from the change in the water density.

In Fig. 6 we plot the effects of a thermocline at $z \simeq 40\,\mathrm{m}$ with a temperature variation from $T_1 = 20°\mathrm{C}$ to $T_2 = 10°\mathrm{C}$ (the values of depth and themperature gradient of the thermocline have been obtained form Madirolas et al., 2017). We observe that a small drop in the tilting ($\Delta\theta \lesssim 1°$) is produced by this temperature gradient. In the same way, we presume that the variations in the salinity will not be considerable in this respect. We consider that a change of tilting of the order of 1° is small in comparison with the error from the *behavioural component* of the tilt swimming that we do not consider here. For example, in Fréon and Misund (1999) the authors mention that physiological changes are produced when fishes go through the thermocline. They detect a drastic decrease of cardiac rhythm when fish carries out vertical excursion. Such decrease will bring a variation in swimming speed and, possibly, a variation in the swim tilt to accommodate the new buoyancy condition. However, the cause of this change is not hydrodynamic but physiological. We call the behavioural component of the tilt swimming to this type of phenomena, and they are not considered in the present hydrodynamic model. Also, we can imagine that the horizontal steady swimming strategy could shift to another swimming strategy when going through the thermocline. This change may again occur because of behavioural reasons and not only from hydrodynamical effects. Certainly, a change in the swimming strategy may introduce bigger changes in the fish tilting than the thermocline effect on the horizontal steady swimming. For example, if the fish chooses different swimming strategies for different depths or times of the day (Huse and Ona, 1996; Paoletti and Mahadevan, 2014). For the aforementioned, we conclude that the presence of such a thermocline will not introduce significant changes in the tilting of hydrodynamic origin.

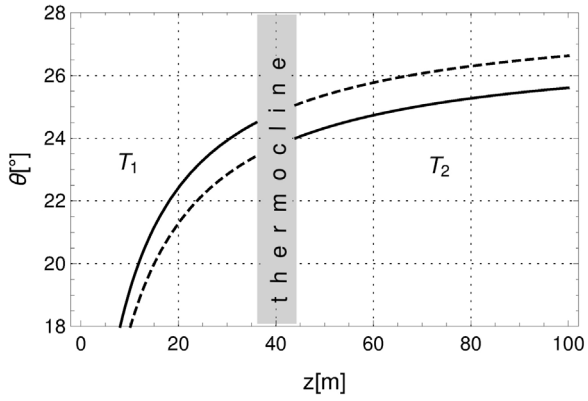

Fig. 6. Variation of $\theta\,[deg.\,]$ when going through the thermocline (solid line) as a function of $z\,[\mathrm{m}]$. The dashed line serves to visualizate which is the $\Delta\theta$ as a function of z when $\Delta T = T_1 - T_2$.

3. An example with Argentine anchovy

In this section we shall study the previous implications for a particular fish: Argentine anchovy. We are particularly interested in this fish because recently in Madirolas et al. (2017) there were reported *in situ* Target Strenght (TS) measurements where they suggested an increasing body tilting behaviour with depth. Furthermore, they suggested a tilting vs depth behaviour by simulating theoretical TS functions for some scenarios of swimbladder contraction and tilt angle distributions. We wish to compare the predicted TS obtained from PSM simulations with the *in situ* acoustic measurements. In doing so, we will use the tilt angle obtained from the hydrodynamic model as input for the mean tilt of simulated average TS. We next give the parameters used in the hydrodynamic model to calculate the tilt angle from Eqs. (9) or (13).

3.1. Hydrodynamic model parameters

Some of the parameters used in the present example correspond to the ones in Madirolas et al. (2017) obtained from X-ray tomography for a representative specimen. On the other hand, we choose standard representative values for the seawater parameters (Table 1).

We adopted the value $\varkappa = 0$ which implies that we are not considering lift generated by the pectoral fins ($L_f = 0$). Moreover, this means the absence of any drag of the fins, $D_f = D_i = 0$ (see Appendix A). The choice of this parameter was made for simplicity reasons given that there are no measurements of $\varkappa$ for this fish. Some typical values of

Table 1
Anatomical fish and sea water physical parameters used in the hydrodynamical model.

Symbol	Parameter	Numerical value
ρ	Water density	$1026\,\mathrm{kg/m^3}$
μ	Water viscosity	$1.8 \times 10^{-3}\,\mathrm{kg/(m\,s)}$
ρ_b	Fish body density	$1060\,\mathrm{kg/m^3}$
ℓ	Fish body length	15 cm
V_{b0}	Sea level body volume	$20\,\mathrm{cm^3}$
V_{sb0}	Sea level swimbladder volume	$0.6\,\mathrm{cm^3}$
r_b	Body transversal radius	0.8 cm
$\varkappa$	Pectorals lift coefficient	0
A_s	Stern area	0
g	Gravity acceleration	$9.81\,\mathrm{m/s^2}$

κ range between π and 2π, in particular for slender aerofoils like NACA 2306, 6306, etc., with $\kappa \simeq 1.4\pi$ or NACA 6506 with $\kappa \simeq 1.2\pi$ (Jacobs et al., 1935; Hoerner and Borst, 1975). If such lift fins contributions are included we found that the tilt drops about 5°. The difficulty of determining the value of this parameter resides primarily on the fact that it depends strongly on the fish behaviour. There is a wide range of possible fin movements: some fishes are able to control every fin ray separately, they can deform the fins or retract them, or rotate the rays at willing (Videler, 1993). Indeed, this correction appears to be meaningful, thus it would be interesting to orient some future investigations in this direction.

3.2. Comparative with acoustic data

Authors in Madirolas et al. (2017) obtained an experimental curve for average acoustic backscattering strength *TS* for the nighttime scattering layer of Argentine anchovy.

$$\mathrm{TS}_{\mathrm{exp}}(\ell, z) = 31.3\log\ell - 79.6 - 4.74\log\left(1 + \frac{z}{10}\right). \tag{15}$$

Furthermore, they used a Prolate Spheroidal Model (PSM) (Prario et al., 2015) to simulate the variation of the average TS with depth z for a distribution function with mean tilt $\bar{\theta}$ and standard deviation SD. In that opportunity, the anatomy of the anchovy swimbladder was obtained from X-ray Computed Tomography (CT scanning). In this work we repeated the same runs of the PSM simulations (with the same parameters, Table 2) as used in Madirolas et al. (2017). In this sense, we considered coherent contributions of the three backscattering sources: the dual-chambered swimbladder and the anchovy body. The TS outputs were averaged over the tilt angle through a gaussian window with mean $\bar{\theta}$ and standard deviation SD. A detail discussion of the TS simulations is given in Appendix B.

If we assume that anchovies are neutrally buoyant near the surface, and considering the loss of buoyancy with depth due to swimbladder compression, a reasonable interpretation of these simulations with the experimental data is that the mean tilt angle increases with depth. Indeed, this is a swimming strategy chosen by fish to avoid sinking. In this work we deduced, using a hydrodynamic picture, some expressions that can give quantitative estimations for these tilt changes with depth variations.

With these ideas we combined the hydrodynamical model of tilted swimming with the PSM simulations. In this sense, we considered that the hydrodynamical prediction of Eqs. (9) or (13), for $\theta(z, v)$, would correspond with the statistical mean tilt angle $\bar{\theta}$. In Fig. 7 we show the results of evolving $\bar{\theta}$ with the hydrodynamic equations for horizontal velocities $v[\ell/s] = 1.5, 2, 2.5$ and using SD = 20°. At first sight when comparing with the experimental function, and assuming that the dispersion in the tilt angle does not change, the simulations would imply that there is a slight decay in the velocity when the tilt changes. Such conclusion is reasonable in the fact that, when tilting, some of the power of swimming is spent propelling water downwards. On the other side, using SD = 10°, we can see in Fig. 8, (left plot), that the experimental curve is much more compatible with such simulation at deeper depths ($\gtrsim$30 m). These results are improved when considering CSP in the simulations (right plot).

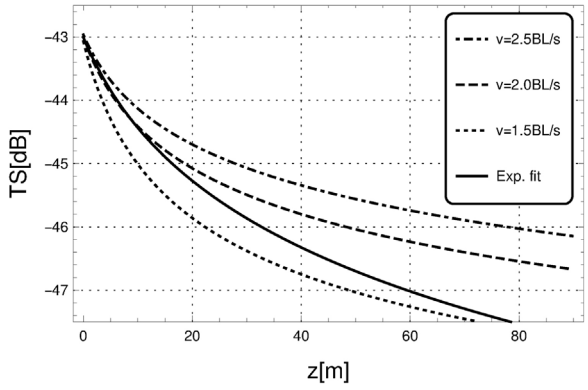

Fig. 7. Average *TS*[dB] vs z[m] obtained from the PSM simulations using the hydrodynamic model for horizontal velocities v[BL/s] = 2.5, 2.0, 1.5. Solid line corresponds with experimental fit, Eq. (15), for Argentine Anchovy.

To conclude, we observe that for shallower depths the hydrodynamics curves are compatible with acoustic data for SD = 20°, while for deeper depths, the tendencies agree with a more polarized swimming, SD = 10° ∼ 15°. We shall interpret this situation in terms of the change of the swimming stability with the depth. If we introduce a small perturbation $\delta\theta$ from an equilibrium tilt θ (with v constant) the corresponding change in the drag δD and the lift δL shall increase for bigger θ. Thus, for the fish to recover the equilibrium, it will need a stronger δT for bigger θ. We show this effect in Fig. 9 where we can observe that the derivative of the thrust T, computed from Eq. (2), it increases practically in the considered tilt range. Yet, there may exist a range of small angles where the derivative is negative, sourced by the drag term proportional to $C_{||}\cos^3\theta$ (see Eq. (25)), which all the same appears to be residual.

4. Discussion

In spite of the substantial influence that fish tilted swimming have on the acoustic backscatter response, direct observations of fish swimming tilt angle are rather scarce. In this way the add-on of the present hydrodynamical model to TS simulations can be used to perform a more physically realistic acoustic modelling.

The present model arises from an attempt to optimize the relation between the simplicity of its formulation and the generality of results. We obtained an analytical model that is applicable to physostomous fish, more specifically to thunniform and carangiform swimmers (Eq. (13)). We highlight the advantage that analytical models show in which the action and relevance of the variables and parameters involved can be explicitly identified. Due to the simplicity of the model we cannot expect to be accurate, but rather approximate, trying to rescue the principal factors that dominate dynamics. However, this fact is not a relevant problem necessarily because tilted swimming usually has a behavioural component not considered in the hydrodynamical model that increases the standard deviation beyond what would be physically expected, making unnecessary more accuracy.

It is a physical fact that a swimming fish generates vortices in its wake (Rosen, 1959; Webb, 1975; Müller et al., 1997; Shadwick et al., 1999; Lauder and Drucker, 2002), so it follows that individuals in a school swimming behind each other will encounter vortices from the propulsive wakes of preceding members. Indeed, fish in schools can benefit from altered flows using two distinct though not mutually exclusive mechanisms: flow refuging and harnessing energy from vortex capture. These mechanisms can theoretically increase the thrust of an individual by tens of percentages without additional energy expenditure. Nevertheless, such schooling altered flows will in principle break down any predictability derived from the steady-flow assumption of individual fish discussed in the present work. In fact, much less is known about effects of hydrodynamics that deviate from steady conditions. Numerous field and laboratory studies have shown that fish can reduce locomotory costs by exploiting turbulence generated by water moving past physical structures or by the propulsive movements of other fishes (Breder, 1965; Weihs, 1973; Herskin and Steffensen, 1998; Hinch and Rand, 1998; Liao et al., 2003b). Under these circumstances, turbulence may be considered a feature of the hydrodynamic environment that is a benefit rather than a constraint. By the way, observations of individual positions in a school have provided useful information, but still almost no hydrodynamic or physiological data exist to evaluate the hypothesis that fish can increase swimming performance by taking

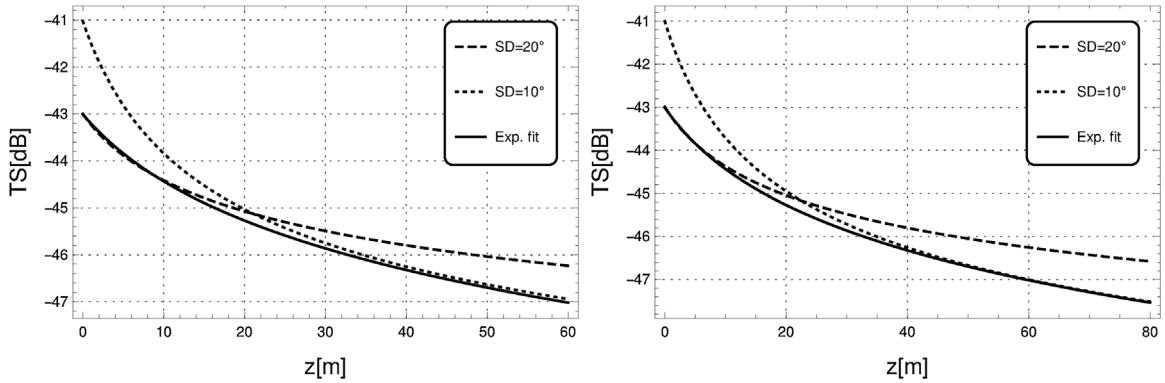

Fig. 8. Average TS[dB] vs z[m] obtained from the PSM simulations using the hydrodynamic model with $SD = 10°$ (dashed) and $SD = 20°$ (dotted) with constant velocity $v = 2.0$ BL/s on the left plot and CSP with initial velocity $v_0 = 2.1$ BL/s on the right plot. Solid line corresponds with experimental fit, Eq. (15), for Argentine Anchovy.

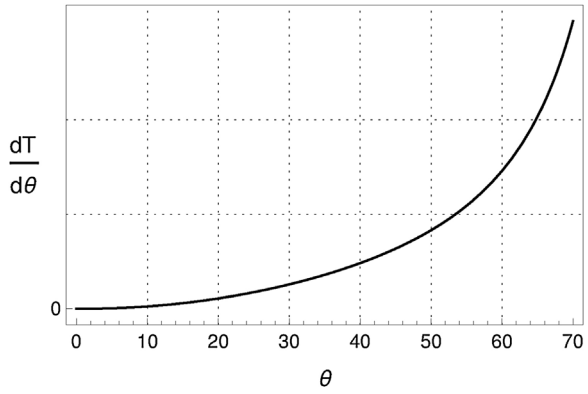

Fig. 9. The derivative of the thrust $dT/d\theta$ computed from Eq. (2) in arbitrary units.

advantage of the wake of other members (Liao, 2007).

We remark, then, that our hydrodynamical model in general will not be applicable for compact fish schools, where the presence of altered flows and vortices dominate the water dynamics. In spite of this, it could happen that disperse slow-moving fish flocks will minimize the presence of turbulence, allowing for our predictions to be appropriate. Yet first our model should be tested and validated against direct observations of individual fish before trying to extend it to fish schools.

This is a new theoretical treatment, and so still suffers from lack of validation with experimental (e.g., flume tank experiments) and in situ optical data. However, as a first approach this validation may also be carried out by numerical simulations that model the complete hydrodynamic picture. For example, this can be applied for thunniform and carangiform swimmers (Sfakiotakis et al., 1999) by introducing the hydrostatics of the open swimbladder. We do expect that corrections may indeed appear to our framework when including the undulatory phenomenology, the thrust generation and the swimming bio-energetics. All the same, there are experimental reports that support our results. In (He and Wardlet, 1986; Svendsen et al., 2005; Nowroozi et al., 2009) they obtained experimental curves that show a decresing of tilt angle with velocity in agree with Eq. (13). Webb (1993) obtain an empirical fitting that relate tilt angle and swimming velocity according to $\theta \propto v^{-1.14\pm0.41}$ for steelhead trout. This result is compatible with our prediction $\theta \sim v^{-1}$ of Eq. (13). Finally, we predict a decrease in the swimming velocity and an increase of tilt angle of horizontally swimming fish that are suitable with the observations of Norwegian herring made by Huse and Ona (1996).

We emphasize that our model is a simplification and therefore has left out some important effects. Our results should be interpreted as mean values that coincide with fish that, under certain conditions, have an average behaviour or swimming strategy that is related to steady horizontal swimming. This hydrodynamical model is not applicable when fish deviate significantly from this behaviour. Indeed, other swimming strategies would surely involve other dynamic equations, maybe involving accelerations and oblique trajectories. A natural generalization of the model should include a rigorous estimation of significant parameters, such as κ in the lift fins; the incorporation of the hydrodynamic aspects of the modes swimming propulsion as well as the comparison of results between different swimming strategies. This last point will be the subject of our next project.

5. Conclusions

We implemented from first principles a model for physostomus fish that describes the relation between hydrodynamical forces and body tilt during stationary swimming velocity at certain depth.

To study swimming stability we took into account thrust, drag and lift forces, and the apparent weight. The last depends on swimbladder volume, for which we adopted Boyle's Law to describe compression at depth. Taking these considerations into account, we obtained an analytical expression for depth as a function of body tilting and swimming velocity. These last variables have a hydrodynamical component considered in the model and a behavioural component that is not considered.

We found that in rather general conditions, for fixed tilting θ, swimming depth z changes hyperbolically as v^{-2}. Moreover, we obtained a useful approximate expression (Eq. (13)) for fish tilting as a function of depth and the swimming velocity that behaves like v^{-1}. Hence, for faster swimming the fish will need less body tilting for a fixed z. To the contrary, more dense fish will need more body tilting to cancel out the extra weight. Additionally, from Eq. (13) one can identify, for each swimming velocity, a maximum tilt $\theta_{\max}$ when $z \gg z_* \simeq 10$ m.

We analysed hydrodynamic changes that a thermocline would produce in fish swimming behaviour. In spite of the presence of the temperature gradient we found that the effects of the thermocline with body tilt are small ($\Delta\theta \approx 1°$ for $\Delta T \approx 10\,^{\circ}$C). Thus, we concluded that the thermocline does not affect fish tilting of hydrodynamic origin significantly. However, there could be changes of tilt swimming of behavioural origin not contemplated in the hydrodynamical model.

The knowledge of body tilt distribution for fish is of utmost importance for fisheries acoustics, given that backscattering strength is mainly originated at the exposed fish area. We tested the present hydrodynamical model and the hypothesis of constant swimming power (CSP) against *in situ TS* measurements and simulated data for Argentine Anchovy (Madirolas et al., 2017). In that case, they commented that the lack of the observed TS with depth could not be explained by

swimbladder compression only, suggesting a behavioural tilting. Thus, in this work, we associated this difference with a quantitative combination of swimbladder compression and body tilting excursion with depth by means of hydrodynamic arguments. From the comparison between the acoustic observation with the PSM simulations combined with the mean tilt angle prediction from the hydrodynamic model, we found that body tilting standard deviation may show a slight decreasing trend with depth unless a different swimming strategy is selected. We gave an interpretation of these results in terms of stability.

Acknowledgements

We wish to thank Adrian Madirolas (INIDEP) for providing us the PSM simulated data needed to compare to our model, for useful discussions in fisheries acoustics and the hospitality we received at INIDEP. We are also grateful with Guido Bacino (CONICET) for discussions and help in oceanography, and Constanza Brasesco (CONICET) for manuscript corrections.

Appendix A. Hydrodynamic forces

In this appendix we shall consider analytical expressions for the drag D and lift L forces. In Fig. 10 we plotted generic solutions for the total D and L that we encountered all through the paper. As we can observe, for small tilt angles the drag force dominates the lift, but for bigger θ they both grow becoming comparable.

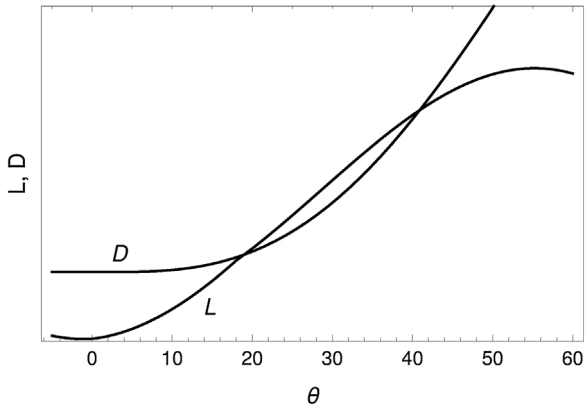

Fig. 10. Generic shape for L and total D in arbitrary units as a function of $\theta[deg.]$.

A.1 Lift force

The lift **L** is produced by the dynamic effect of the water acting on the fish. It appears when an object changes the direction of flow of the water. This force is the hydrodynamic force orthogonal to the swimming direction. It helps to swim at a certain depth by stabilizing with the negative buoyant force, reaching to supply up to half of the force necessary to avoid sinking (Nowroozi et al., 2009). We shall consider two sources of lift force, from the pectoral fins L_f and from the fish body L_b, thus the total lift is given by

$$L = L_b + L_f = \frac{1}{2}\rho v^2 (A_r\ C_{\mathrm{Lb}} + S_r\ C_{\mathrm{Lf}}) \tag{16}$$

where A_r and S_r are the reference areas of the body and the fins, respectively. And C_{Lb} and C_{Lf} are dimensionless lift coefficients that relate the fluid variables ρ and v to the lift force on the body and the fins, respectively.

A.1.1 Body lift

Jorgensen (1973) obtained some heuristic and theoretical formulas for predicting hydrodynamic forces on a streamlined body in terms of the angle of attack. The original formulas give the axial (C_A) and normal (C_N) coefficients with respect to the fish length. Yet, for our calculations we need the lift and drag coefficients, so we performed a rotation of the coordinate system at an angle θ so as to relate C_A and C_N with C_L and C_D. Thus for the lift coefficient we obtain

$$\begin{aligned} C_{\mathrm{Lb}} &= C_N \cos\theta - C_A \sin\theta, \\ &= -C_{\parallel}(v)\frac{A}{A_r}\cos^2\theta \sin\theta + C_s \frac{A_s}{A_r}\sin 2\theta \cos\theta \cos\frac{\theta}{2} + C_{\perp}(v)\frac{A_p}{A_r}\sin^2\theta\cos\theta, \end{aligned} \tag{17}$$

where C_s is usually referred to as the apparent mass factor that depends on the ratio L/r, in our case $C_s \sim 1$ for streamlined bodies, A_s is the area of the body stern, A_r is the reference area, A_p is the planform area of the fish body (the maximum projected area), A is the body or wetted area. Note that the global factor A_r^{-1} will simplify with the factor A_r in Eq. (16).

$C_{\parallel}$ is the total axial drag at zero angle of attack which is composed by friction and pressure contributions. To estimate the value of the friction through the coefficient C_{fric} we need to express it in terms of the Reynolds number (Webb, 1975), defined by

$$R_\ell = \frac{\rho \ell v}{\mu}, \tag{18}$$

where ρ is the water density, ℓ is the fish large, v the fish velocity and μ the water viscosity. Essentially there are three types of flows depending on the Reynolds number with their respective functions of the friction coefficient (Webb, 1975),

$$C_{\text{fric},b} = \begin{cases} 1.33R_\ell^{-\frac{1}{2}}, & \text{LAMINAR} \\ 0.072R_\ell^{-\frac{1}{5}} - 1700R_\ell^{-1}, & \text{TRANSITIONAL} \\ 0.072R_\ell^{-\frac{1}{5}}, & \text{TURBULENT} \end{cases} \tag{19}$$

These formulas give an estimation of the friction coefficient in the laminar, transitional and turbulent flow regimes respectively. The change of the laminar to transitional regimes is governed by a Reynolds number around 5×10^5. In our case, $R_\ell < 10^4$, therefore we shall work in the laminar regime.

On the other hand, for streamlined bodies the pressure component can be related to the friction coefficient and to the ratio between the maximum diameter $2r$ and the length ℓ,

$$C_{\text{press},b} = C_{\text{fric},b} G(2r/\ell), \tag{20}$$

where $G(x) = 1.5x^{3/2} + 7x^3$. With these expressions we can define the total axial drag as

$$C_\parallel = C_{\text{fric},b} + C_{\text{press},b} = C_{\text{fric},b}(1 + G). \tag{21}$$

$C_\perp$ is the cross-flow drag coefficient for a finite cylinder section, we shall use the empirical formula, $C_\perp(v) = \eta(1 + 10R_N^{-2/3})$ proposed by White (White, 1991) and Vogel (Vogel, 1996) with a *normal Reynolds number* $R_N(\theta) = R_{2r}\sin\theta = 2r\rho v \sin\theta/\mu$. We have introduced the correction factor η for finite cylinder in the formula which in our case ~ 0.82 (Jorgensen, 1973). We have tested that in the range of Reynolds number of interest, the variation of $C_\perp$ with the velocity introduces minimal changes to the final result. Thus, we keep a constant coefficient slightly bigger than η,

$$C_\perp(v) \sim \overline{C}_\perp \gtrsim \eta. \tag{22}$$

The first term in (17) corresponds to lift generated by a finite body stern area and may in general be small for streamlined fishes. The second term produces a small negative lift coming from the frontal area of the head. Lastly, in general the third term produces most of the lift that comes from the longitudinal body area exposed to cross-flow when tilting is present. These three terms are shown in the left plot of Fig. 11, while in the right plot we compare the angular dependence of body and fins lift.

A.1.2 Fins lift

We shall use for the fins, the usual simplified expression for hydrofoils (Webb, 1975),

$$C_{\text{Lf}} = \kappa \sin\alpha, \tag{23}$$

with α the angle of attack with respect to the flow direction and κ a constant that depends on the form of the fins. For a hydrofoil there exists a critical angle α_{crit} for which above of this value the flow becomes strongly distorted and the value of C_L rapidly decays, in this situation it is said that the hydrofoil stalls. In this work we shall consider that the fish can control the stall situation by changing the angle of attack of the pectoral fins. In this sense, we assume that $\alpha = \theta$ for $\theta < \alpha_{\text{crit}} \sim \pi/10$, while for $\theta > \alpha_{\text{crit}}$ then $\alpha = \alpha_{\text{crit}}$ and the coefficient remains almost constant in a way that maximizes the lift force of the fins [1] (see Fig. 11).

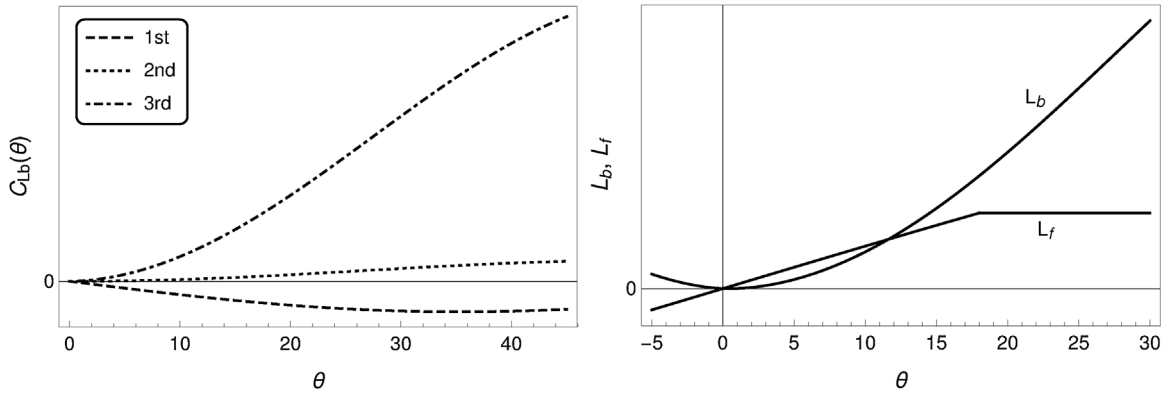

Fig. 11. Left plot: the different lift terms of Eq. (17) in arbitrary units as a function of θ[*deg.*]. Right plot: The angular dependence of body and fins lift of Eq. (16) in arbitrary units as a function of θ[*deg.*].

A.2 Drag force

The drag **D** is the resistance force caused by the motion of a body through a fluid. The drag force always opposes to the fish velocity. We shall study the drag on the pectoral fins acting as hydrofoils and on the rest of the body. These are also given by a similar expression as for the lift force,

$$D = D_b + D_f = \frac{1}{2}\rho v^2(A_r C_{\text{Db}} + S_r C_{\text{Df}}) + D_i, \tag{24}$$

where C_{Db} and C_{Df} are the body and fins drag coefficients, respectively, and D_i is the induced drag that we shall analyse later in this section.

[1] Indeed, a simpler assumption would be to consider a constant lift coefficient that maximizes the lift force, $C_{\text{Lf}} \lesssim \kappa \sin\alpha_{\text{crit}}$.

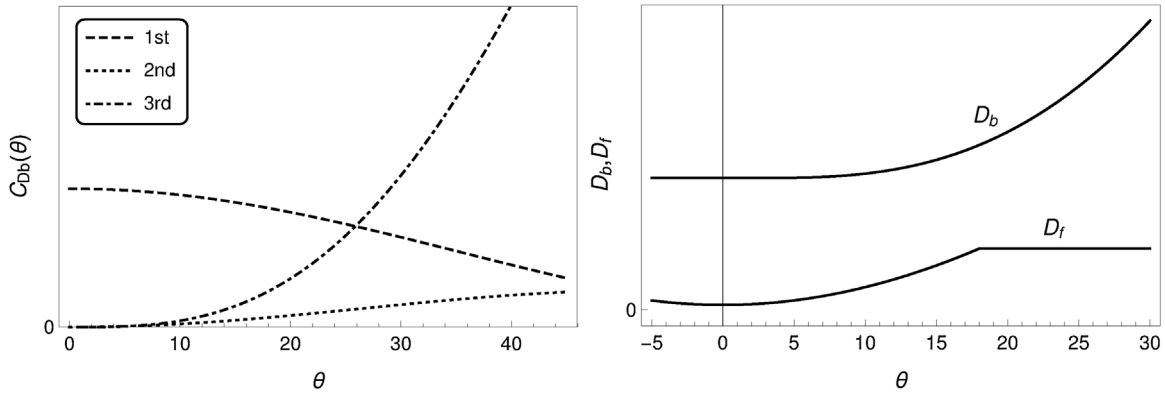

Fig. 12. Left plot: the different drag terms of Eq. (25) in arbitrary units as a function of $\theta\,[deg.\,]$. Right plot: The angular dependence of body and fins drag of Eq. (24) in arbitrary units as a function of $\theta\,[deg.\,]$.

A.2.1 Body drag

Analogously to how the body lift coefficient was written, the body drag coefficient is related to C_A and C_N in the following way,

$$C_{\mathrm{Db}} = C_N \sin\theta + C_A \cos\theta, \tag{25}$$

$$= C_s \frac{A_s}{A_r} \sin 2\theta \sin\theta \cos\frac{\theta}{2} + C_{\perp} \frac{A_p}{A_r} \sin^3\theta + C_{||} \frac{A}{A_r} \cos^3\theta.$$

The coefficients C_s, $C_{\perp}$ and $C_{||}$ were defined previously in the body lift section. These three terms are shown in the left plot of Fig. 12, while in the right plot we compare the angular dependence of body and fins drag.

A.2.2 Fins drag

The drag of the fins will be given by the sum of three terms: the friction $D_{\mathrm{fric},f}$ and pressure drag $D_{\mathrm{press},f}$, which speak of the direct interaction of the fluid on the fins, and the induced drag D_i, which comes whenever lift is present at hydrofoils.

The first two terms will have a friction $C_{\mathrm{fric},f}$ and a pressure component $C_{\mathrm{press},f}$ defined by a Reynolds number calculated with the fins chord c and span b, thus we write,

$$D_{\mathrm{fric},f} + D_{\mathrm{press},f} = \frac{1}{2}\rho v^2 (4\mathrm{bc} C_{\mathrm{fric},f} + 2\mathrm{bc}\sin\theta C_{\mathrm{press},f}), \tag{26}$$

where the area 4bc corresponds to the total wetted area of both pectoral fins, while $2\mathrm{bc}\sin\theta$ is the area frontal to the flow direction for an angle of attack $\alpha = \theta$. Moreover, we have assumed that the contribution of the transversal area of the fins is negligible.

The magnitude of the pressure coefficient for a hydrofoil can be approximately related to the *thickness ratio* τ (Webb, 1975),

$$C_{\mathrm{press},f} = C'_{\mathrm{press},f} + 0.0056 + 0.01\tau + 0.1\tau^2, \tag{27}$$

where $C'_{\mathrm{press},f}$ is the pressure component associated to the relative camber (Webb, 1975). For our calculations we shall assume that the fins thickness ratio is very small $\tau \ll 1$, and that the camber is small also, thus $C_{\mathrm{press},f} \simeq 0.0056$. Furthermore, we obtain that the pressure drag on the pectoral fins will be much smaller than the friction drag.[2]

The third drag term is a consequence of the work that the hydrofoil makes on the fluid to push it downwards. Thus, D_i is associated to the reaction of giving kinetic energy to the fluid by the fins. We have used an estimate given by momentum-jet theory (Norberg, 1990),

$$D_i = \frac{2}{\pi b^2 \rho v^2} L_f^2. \tag{28}$$

Using expression (24) we can deduce a coefficient $C_{D,i} \propto \frac{C_L^2}{\mathrm{AR}}$, where $\mathrm{AR} = b^2/S_f$ is the aspect ratio given by the relation between the fin span and the fin area.

A.3 Demonstration of the factorization $v^2 f_1(\theta)$

Let us consider the expression $D(\theta, v)\tan\theta + L(\theta, v)$ of Eq. (10). If we take into account the corresponding term $C_{||}$ of L_b and the respective of D_b, they cancel each other. Furthermore, as we discussed in (A.1.1) we can consider a constant $\overline{C_{\perp}}$. If we additionally consider that the viscous and pressure drag contribution from the fins is negligible and the remaining lift and drag terms are all proportional to v^2, then we can factorize a global factor as in Eq. (10).

Appendix B. Prolate spheroidal acoustic model (PSM)

The far field backscattered sound wave of individual fish is defined (at linear order) through the coherent sum of the backscattering amplitude functions of swimbladder f_{sb} (soft spheroid) and fish body f_b (fluid spheroid) (Prario et al., 2015). Argentine anchovy posses a dual-chambered

[2] For a flat plate normal to the incident flow the drag force is mostly from pressure forces, and then it is independent of R_ℓ, however this corresponds to a critical situation where the fish fins would have an angle of attack $\alpha \lesssim 90°$ which we consider a rather odd situation for steady swimming.

Table 2
Fish body and dual-chambered swimbladder parameters used in PSM simulations. The selected anchovy specimen (total length = 14.7 cm) has been previously adapted to the hydrostatic pressure conditions of sea surface.

Fish body	
Total length	14.7 cm
Standard length	12.1 cm
Max. width	1.6 cm
Max. height	2.0 cm
Volume	26.1cm^3
Surface (total)	65.5cm^2
Equivalent spheroid width[a]	2.0 cm
Sb-anterior chamber	
Max. length	1.27 cm
Max. width	0.49 cm
Max. height	0.53 cm
Volume	0.12cm^3
Surface (total)	1.63cm^2
Surface (dorsal)	0.61cm^2
Equivalent spheroid width[b]	0.38 cm
Vertical offset[c]	0.10 cm
Horizontal offset[c]	1.4 cm
Longitudinal angle	5°
Sb-posterior chamber	
Max. length	2.7 cm
Max. width	0.55 cm
Max. height	0.70 cm
Volume	0.42cm^3
Surface (total)	4.12cm^2
Surface (dorsal)	2.37cm^2
Equivalent spheroid width[b]	0.70 cm
Vertical offset[c]	0.35 cm
Horizontal offset[c]	−0.70 cm
Longitudinal angle	5°

[a] Obtained for spheroid volume = body volume and spheroid length = body std. length.
[b] Obtained for spheroid dorsal surface area = sb dorsal surface area and spheroid length = sb length.
[c] Coordinates of the geometrical centroid of the chamber relative to the centroid of the fish body. From Madirolas et al. (2017).

swimbladder, thus, for the simulation we considered the contribution of both independent sources (Madirolas et al., 2017). The total backscattering cross-section is then computed as,

$$\sigma_{\mathrm{bs}} = |f_{\mathrm{sb1}} e^{2i\frac{c_0}{c_1}\mathbf{k}\cdot\boldsymbol{\delta_1}} + f_{\mathrm{sb2}} e^{2i\frac{c_0}{c_2}\mathbf{k}\cdot\boldsymbol{\delta_2}} + f_b|^2, \tag{29}$$

with sound velocities inside the swimbladder chambers $c_1 = c_2$. The coherent sum of the sources is performed by the complex nature of backscattering functions. Moreover, exponential phase factors are important because they account for the spatial displacements between the spheroids centers.

In the PSM picture the fish body parts are approximated by equivalent spheroids. Therefore, backscattering functions are expanded in prolate spheroidal functions so as to easily fulfil with the boundary conditions. Moreover, anchovy morphometry was obtained by Madirolas et al. (2017) from CT scanning. In the present work we repeated the same modelling parameters (see Table 2). These consisted on assuming that the widths of soft spheroids are such that the measured dorsal area of swimbladder chambers coincide with that of their equivalent spheroids. Also, the lengths of the soft spheroids would be equal to the corresponding swimbladder chamber. On the other side, the width of the fluid spheroid was chosen so as to keep the same volume with the fish body, while lengths stayed equal.

In order to study the vertical *TS* variations, we assumed Boyle's Law for volume changes of the swimbladder chambers with hydrostatic pressure. However, swimbladder contractions could be anisotropic. Thus, we adopted the following equations to describe changes in the gas-filled spheroids dimensions (Gorska and Ona, 2003),

$$a_{\mathrm{sb}}(z) = a_{\mathrm{sb0}}\left(1 + \frac{z}{z_*}\right)^{-\alpha}, \tag{30}$$

$$\ell_{\mathrm{sb}}(z) = \ell_{\mathrm{sb0}}\left(1 + \frac{z}{z_*}\right)^{-\beta}, \tag{31}$$

where a_{sb0} and ℓ_{sb0} are the spheroids diameter and length at sea surface, respectively. Moreover, to comply with Boyle's Law, the exponents should satisfy the constraint equation $2\alpha + \beta = 1$. Isotropic compression then implies $\alpha = \beta = 1/3$, while pure transverse compression is achieved for $\alpha = 1/2$ and $\beta = 0$. All simulations were carried out using pure transverse compression that, as was suggested by Madirolas et al. (2017), would be

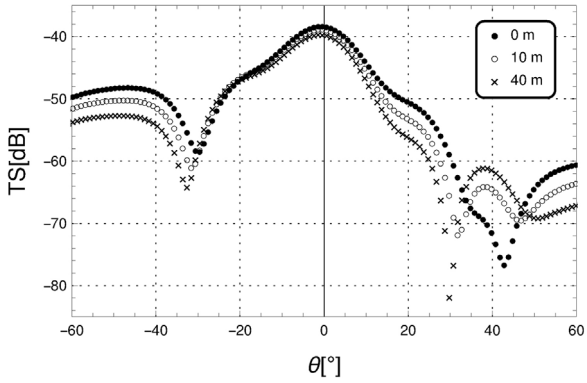

Fig. 13. Fish total sound scattering of PSM simulation of the sound scattering function at 38 kHz for an anchovy of total length ℓ[cm] = 14.7 at depths z[m] = 0, 10, 40..

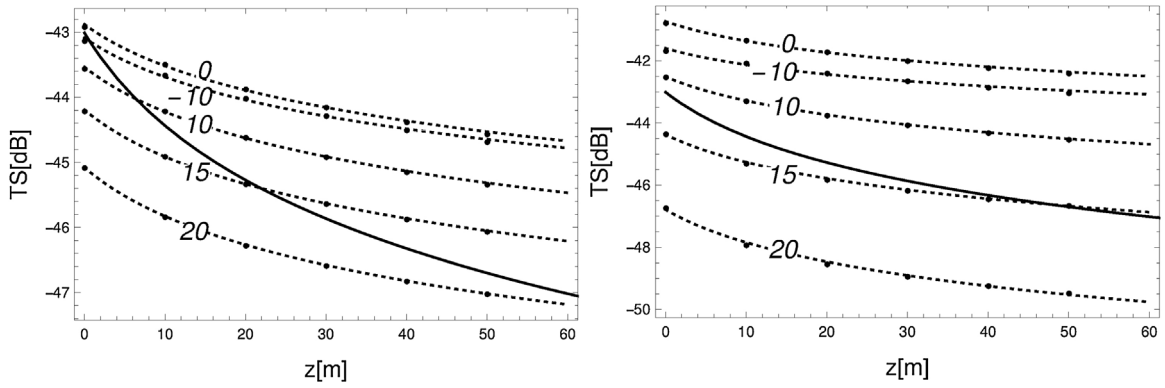

Fig. 14. Averaged TS [dB] points for z [m] = 0, 10, 20, 30, 40, 50 obtained from PSM simulation using Boyle's Law with pure transverse compression with $SD = 20°$ on the left plot and $SD = 10°$ on the right plot. Fitting functions appear in dashed lines. Experimental fit appears in solid line.

compatible with a tilted swimming behaviour of anchovies with depth. In this same work they identified that an isotropic compression yields incompatible results, while there exists a marginal intermediate compression scenario ($\alpha = 0.37$ and $\beta = 0.26$) that would indicate no tilting behaviour at all. At the moment these exponents are fairly unknown for Argentine anchovy. However, for instance, herring morphometry of the swimbladder compression with varying pressure was examined using magnetic resonance imaging by Fässler et al. (2009). In this sense, to completely validate the present framework, analogous experiments should be carried out for anchovies in the future.

In Fig. 13 we plotted TS outputs for three different depths (z[m] = 0, 10 and 40) obtained from PSM simulations. It can be seen that the TS function is peaked at $\theta \simeq -5°$, because we used a 5° inclination of the swimbladder longitudinal axis relative to the fish body length.

To compare with experimental fits, we averaged the simulated backscattering cross-sections over the tilt angle. The averaging was done through a gaussian window with mean $\bar{\theta}$ and standard deviation SD. In Fig. 14 we plotted points for depths $z[m]$ = 0, 10, 20, 30, 40, 50 of averaged TS, for SD = 20° (left plot) and SD = 10° (right plot); and for mean angles $\bar{\theta} = -10°, 0°, 10°, 15°, 20°$. In addition, the curves are best fits to the two parameter function $TS_{\text{sim}}(\bar{\theta}, \text{SD}; z) = A(\bar{\theta}, \text{SD}) + 10\gamma(\bar{\theta}, \text{SD})\log(1 + (z/10))$. We note that the fitting parameters A and γ will depend solely on the averaging variables $\bar{\theta}$ and SD. As a reference, we included the experimental fit function $TS_{\text{exp}}(\bar{L}, z)$ with $\bar{L} = 14.7$ cm. As going to deeper depths, this function intersects different simulation curves TS_{sim}.

References

Alexander, R.M., 1990. Am. Zool. 30, 189.
Blaxter, J.H.S., Batty, R.S., 1984. J. Mar. Biol. Assoc. UK 64, 441.
Blaxter, J.H.S., Hunter, J.R., 1982. Adv. Mar. Biol. 20, 1.
Brawn, V.M., 1962. J. Fish. Res. Board Canada 19, 635.
Breder, C.M., 1965. Zoologica 50, 97.
Evans, J.P., 2003. Dynamics modelling and performance evaluation of an autonomous underwater vehicle. McGill University, Quebec, Canada (Master of Engineering thesis).
Fässler, S.M.M., Fernandes, P.G., Semple, S.I.K., Brierley, A.S., 2009. J. Fish Biol. 74, 296.
Federal Aviation Administration, Helicopter Flying Handbook. U.S. Department of Transportation, EEUU. Download from: http://www.faa.gov/regulations_policies/handbooks_manuals/aviation/helicopter_flying_handbook/.
Foote, K.G., 1980a. J. Acoust. Soc. Am. 67, 2084.
Foote, K.G., 1980b. J. Cons. Int. Explor. Mer. 39, 193.
Fréon, P., Misund, O.A., 1999. Dynamics of Pelagic Fish Distribution and Behaviour: Effects on Fisheries and Stock Assessment. Fishing News Books, Cambridge, UK.
Gilles, R. (Ed.), 1991. Advances in Comparative and Environmental Physiology, vol. 8 Springer-Verlag, Berlin Heidelberg, Germany.
Gorska, N., Ona, E., 2003. ICES J. Mar. Sci. 60, 548.
Hazen, E.L., Horne, J.K., 2003. ICES J. Mar. Sci. 60, 555.
He, P., Wardlet, C.S., 1986. J. Fish Biol. 29 (Suppl. A), 223.
Herskin, J., Steffensen, J.F., 1998. J. Fish Biol. 53, 366.
Hinch, S.G., Rand, P.S., 1998. Can. J. Fish. Aquat. Sci. 55, 1821.
Hoerner, S.F., Borst, H.V., 1975. Fluid-dynamic Lift: Practical Information on Aerodynamic and Hydrodynamic Lift, Second Edition. EEUU, U.S. Navy, Brick Town, NJ.
Huse, I., Ona, E., 1996. ICES J. Mar. Sci. 53, 863.
IOC, SCOR, IAPSO, 2010. The international thermodynamic equation of seawater – 2010: Calculation and use of thermodynamic properties. Intergovernmental Oceanographic Commission, Manuals and Guides. UNESCO.
Jacobs, E.N., Ward, K.E., Pinkerton, R.M., 1935. National advisory committee for aeronautics. The characteristics of 78 related airfoil sections from testsin the variable density wind tunnel. R. 460. EEUU, Washington, DC.
Jorgensen, L.H., 1973. Prediction of static aerodynamic characteristics for space-shuttle-like and other bodies at angles of attack from 0° to 180°. National Aeroacoustic and Space Administration (NASA), TN D-6996. EEUU, Washington, DC.
Kang, D., Mukai, T., Iida, K., Hwang, D., Myoung, J.-G., 2005. ICES J. Mar. Sci. 62, 779.
Lauder, G.V., Drucker, E.G., 2002. News Physiol. Sci. 17, 235.
Liao, J.C., Beal, D.N., Lauder, G.V., Triantafyllou, M.S., 2003b. J. Exp. Biol. 206, 1059.

Liao, J.C., 2007. Philos. Trans. R. Soc. B 362, 1973.
Lighthill, J., 1960. J. Fluid Mech. 9, 305.
Lighthill, J., 1971. Proc. R. Soc. Lond. B 179, 125.
Madirolas, A., Membiela, F.A., Gonzalez, J.D., Cabreira, A.G., dell'Erba, M.G., Prario, I.S., Blanc, S., 2017. ICES J. Mar. Sci. 74, 1408.
McNeill, A., 1982. Locomotion of Animals. Blackie & Son Limited, Glasgow, Scotland.
McQuinn, I.H., Winger, P.D., 2003. ICES J. Mar. Sci. 60, 575.
Morrissey, J., Sumich, J.L., Pinkard-Meier, D.R., 2016. Introduction to the Biology of Marine Life, Eleventh Edition. Jones & Bartlett Learning, Burlington, MA EEUU.
Müller, U.K., Van den Heuvel, B., Stamhuis, E.J., Videler, J.J., 1997. J. Exp. Biol. 200, 2893.
Nakken, O., Olsen, K., 1977. Rapp. P.-V. Riun. Cons. Int. Explor. Mer. 170, 52.
Norberg, U.M., 1990. Vertebrate flight. Mechanics, physiology, morphology, ecology and evolution. Zoophysiology 27 Springer-Verlag, Berlin, Heidelberg, Germany.
Nero, R.W., Thompson, C.H., Jech, J.M., 2004. ICES J. Mar. Sci. 61, 323.
Nowroozi, B.N., Strother, J.A., Horton, J.M., Summers, A.P., Brainerd, E.L., 2009. Zoology 112, 393.
Paoletti, P., Mahadevan, L., 2014. Proc. R. Soc. Lond. A 470, 20130535.
Prario, I.S., Gonzalez, J.D., Madirolas, A., Blanc, S., 2015. Acta Acust. Unit. Acust. 101, 1.
Rosen, M.W., 1959. Nav. Ordinance Test Station Tech. Paper 2298. pp. 1.
Schultz, W.W., Webb, P.W., 2002. Integr. Compar. Biol. 42, 1018.
Sfakiotakis, M., Lane, D.M., Davies, J.B.C., 1999. IEEE J. Ocean. Eng. 24 (2), 237.
Shadwick, R.E., Katz, S.L., Korsmeyer, K.E., Knower, T., Covell, J.W., 1999. J. Exp. Biol. 202, 2139.
Shadwick, R.E., Lauder, G.V. (Eds.), 2006. Fish Biomechanics, vol. 23 Elsevier Academic Press, Boston EEUU.
Strand, E., Jørgensen, C., Huse, G., 2005. Ecol. Model. 185, 309.
Svendsen, J.C., Koed, A., Lucas, M.C., 2005. J. Fish Biol. 66, 572.
Talley, L., Pickard, G., Emery, W., Swift, J., 2011. Descriptive Physical Oceanography. An Introduction, Sixth Edition. Elsevier Academic Press, Oxford, UK.
Tanaka, H., Takagi, Y., Naito, Y., 2001. J. Exp. Biol. 204, 3895.
Taylor, G.K., Triantafyllou, M.S., Tropea, C. (Eds.), 2010. Animal Locomotion. Springer-Verlag, Berlin Heidelberg, Germany.
Videler, J.J., 1993. Fish Swimming. Springer-Science + Business Media, Berlin, Heidelberg, Germany.
Vogel, S., 1996. Life in Moving Fluids: The Physical Biology of Flows, Second Edition. Princeton University Press, New Jersey EEUU.
Webb, P.W., 1975. Hydrodynamics and energetics of fish propulsion. Bulletin of the Fisheries Research Board of Canada, vol. 190, Ottawa, Canada.
Webb, P.W., 1988. Am. Zool. 28, 709.
Webb, P.W., 1993. J. Fish Biol. 43, 687.
Weihs, D., 1973. Nature 241, 290.
White, F.M., 1991. Viscous Fluid Flow, Second Edition. McGraw-Hill, Inc., New York EEUU.
Wilga, C.D., Lauder, G.V., 2000. J. Exp. Biol. 203, 2261.